frontiers | Frontiers in Astronomy and Space Sciences

TYPE Mini Review
PUBLISHED 04 March 2024
DOI 10.3389/fspas.2024.1346820

OPEN ACCESS

EDITED BY
Luis Arturo Urena-Lopez,
University of Guanajuato, Mexico

REVIEWED BY
Ricardo Becerril,
Michoacana University of San Nicolás de Hidalgo, Mexico
Ana Aurelia Avilez Lopez,
Benemérita Autonomous University of Puebla, Mexico

*CORRESPONDENCE
Juan Carlos Degollado,
jcdegollado@ciencias.unam.mx

RECEIVED 30 November 2023
ACCEPTED 31 January 2024
PUBLISHED 04 March 2024

CITATION
Bautista B and Degollado JC (2024), Static axion stars revisited.
Front. Astron. Space Sci. 11:1346820.
doi: 10.3389/fspas.2024.1346820

Static axion stars revisited

Brandon Bautista and Juan Carlos Degollado*

Instituto de Ciencias Físicas, Universidad Nacional Autónoma de México, Cuernavaca, Mexico

We consider static solutions to the spherically symmetric Einstein-scalar field systems with an axion potential known as axion stars, originally described by Guerra et al., JCAP (2019, 09 (09)). We construct numerically families of axion stars in the ground state, for different values of the decay constant f_a. It is shown that the existence diagram becomes richer than the mini-boson star case, and several regions of stability appear as the value of f_a decreases, yielding to more massive configurations with larger compactness. Some intrinsic properties, such as isotropy and compactness of such stars, are also discussed. Finally, we describe the motion of test particles around these objects.

KEYWORDS

boson stars, compact object, black holes, general relativity, scalar fields

1 Introduction

Bosonic stars are formed when the density of bosons in a region of space becomes high enough to allow them to gravitationally attract each other and form a self-gravitating configuration overcoming their quantum-mechanical repulsion (Kaup, 1968; Ruffini and Bonazzola, 1969; Mielke and Scherzer, 1981; Colpi et al., 1986; Seidel and Suen, 1990; Mielke and Schunck, 2000; Steven, 2012). Several types of bosonic stars have been proposed, depending on the type of boson involved. These include vector bosonic fields known as Proca stars (Brito et al., 2016; Herdeiro et al., 2019), oscillations (Seidel and Suen, 1991; Alcubierre et al., 2003) or Q-balls (Alexander and Shaposhnikov, 1998; Enqvist and McDonald, 1998). One the simplest configurations are boson stars with a complex scalar field (Jetzer, 1992). Interest in these self-gravitating objects has recently increased due to developments in particle physics and cosmology, suggesting that in the early stages of the universe, bosonic stars may have formed out of fundamental scalar fields and could play a role in understanding the origin of dark matter (Matos and Arturo Urena-Lopez, 2000; Matos et al., 2000; Matos and Arturo Urena-Lopez, 2001; Matos and Arturo Urena-Lopez, 2002; Marsh and Ferreira, 2010; Marsh and Pop, 2015; Marsh, 2016). Among the myriad of candidates proposed to explain this cosmic enigma, axions have emerged as one of the leading candidates to explain the nature of dark matter in the universe (Peccei and Quinn, 1977; Matos and Arturo Urena-Lopez, 2007; Matos et al., 2008; Arvanitaki et al., 2010; Arvanitaki and Dubovsky, 2011; Marsh and Silk, 2014; Porayko and Postnov, 2014; Schive et al., 2014; Sikivie, 2014; Marsh and Pop, 2015; Marsh, 2016). Axion particles were originally proposed in the 1970s as a possible solution to the strong CP problem in particle physics and are the best motivated candidates because of naturally suppressed CP violation in the strong nuclear force. The fundamental theory for the axion field is a renormalizable extension of the standard model in which the Peccei–Quinn symmetry is broken spontaneously by the ground state of a scalar field.

After the original proposal, axion can refer to any low-mass spin-zero particle characterized by a periodic self-interaction potential (Graham et al., 2015; Caso et al., 2018). String theory, for instance, provides grounds for considering the existence of numerous axions with masses spanning several orders of magnitude, and such possibility

has been referred as the *Axiverse* (Arvanitaki et al., 2010; Di Luzio et al., 2020), and the observational consequences of these axions on astrophysical black holes through the Penrose superradiance process have been explored (Arvanitaki and Dubovsky, 2011; Brito et al., 2015). Additionally, extremely light bosonic particles, with masses of the order of 10^{-22} eV, as a candidate for dark matter, have been discussed (Arturo Ureña-López and Matos, 2000; Matos et al., 2000; Matos and Arturo Urena-Lopez, 2007; Lam et al., 2017). Astrophysical constraints coming from the mechanism of cooling of stars due to the emission of axions provide a lower bound on the axion decay constant of the order of $f_a \geq 3\times 10^9$ GeV. On the other hand, the cosmological constraint in the early universe provides a bound of the order of $f_a \leq 10^{12}$ GeV (Marsh, 2016).

Due to the bosonic nature, axions can form a Bose–Einstein condensate (BEC), whose collective behavior can be slightly different compared to an ideal gas of bosons. In this work, we focus on the case of static axion stars, which are spherically symmetric self-gravitating solutions for a scalar field with a periodic potential. Axion boson stars were first studied by Guerra et al. (2019) and later generalized to include rotation by Delgado et al. (2020) and Zeng et al. (2023). More recently, the fermion–axion system has also been studied by Zeng et al. (2021) and Di Giovanni et al. (2022).

We begin by describing the set up to construct self-gravitating axion stars in Einstein theory and provide some basic definitions. We focus on isolated axion stars and summarize some basic features of the equations. Then, we construct families of spherically symmetric solutions with different values of the decay constant f_a and describe some of their properties. Finally, we discuss the motion of test particles, both null and massive, moving in the vicinity of the central object.

2 Axion stars

2.1 Field equations

We consider a complex scalar field minimally coupled to gravity with an action given by

$$S=\int d^4x\sqrt{-g}\left(-\frac{R}{\kappa}+g^{\mu\nu}\nabla_\mu\Phi^*\nabla_\nu\Phi+V(|\Phi|^2)\right), \tag{2.1}$$

where R represents the Ricci scalar, $g=\det(g_{\mu\nu})$, $\kappa=16\pi$, Φ represents the scalar field, and the star stands for the complex conjugate. V represents the self-interacting potential. The variation of the action 2.1 with respect to the metric tensor $g_{\mu\nu}$ leads to Einstein's equations.

$$R_{\mu\nu}-\frac{1}{2}Rg_{\mu\nu}=\kappa T_{\mu\nu}, \tag{2.2}$$

where the stress–energy tensor is given by

$$T_{\mu\nu}=\frac{1}{2}\left[\nabla_\mu\Phi^*\nabla_\nu\Phi+\nabla_\mu\Phi\nabla_\nu\Phi^*\right]-\frac{1}{2}g_{\mu\nu}\left[\nabla^\alpha\Phi^*\nabla_\alpha\Phi+V(|\Phi|^2)\right]. \tag{2.3}$$

The conservation of energy applied to the stress–energy tensor (2.3) reduces to the equation

$$\left(\Box-\frac{dV}{d|\Phi|^2}\right)\Phi=0 \tag{2.4}$$

and its complex conjugate, where $\Box\Phi=g^{\mu\nu}\nabla_\mu\nabla_\nu\Phi$.

2.2 Spherical symmetry

We are interested in static spherically symmetric spacetimes, so we assume the metric can be written as

$$ds^2=-\alpha(r)^2dt^2+a(r)^2dr^2+r^2d\Omega^2, \tag{2.5}$$

where $d\Omega^2=d\theta^2+\sin^2\theta d\varphi^2$ is the metric defined on the two-sphere. In order to construct stationary configurations, we assume a scalar field with a time harmonic dependence of the form

$$\Phi(r,t)=\phi(r)e^{-i\omega t}. \tag{2.6}$$

As described in the work of Guerra et al. (2019), axion stars are constructed with the potential

$$V=\frac{2\mu^2f_a^2}{B}\left[1-\sqrt{1-4B\sin^2\left(\frac{\phi}{f_a}\right)}\right], \tag{2.7}$$

where $B=0.22$ is a numerical factor that depends on the mass of the up and down quarks and μ is identified as the mass of the particles. In the limit $f_a\gg\phi$, the leading term in the power series of the potential leads to a potential with a quartic self-interaction of the form

$$V(\phi)\approx\mu^2\phi^2-\frac{\hbar\mu^2}{f_a^2}\left(\frac{3B-1}{12}\right)\phi^4. \tag{2.8}$$

From 2.8 we thus expect, the major contributions of the periodic potential appear in the limit of small f_a. With the ansatz for metric 2.5 and form 2.6 of the field, the Einstein-scalar field system 2.2, 2.4, 2.7 in spherical symmetry becomes

$$\frac{1}{\alpha}\frac{d\alpha}{dr}=\frac{a-1}{2r}-\frac{r\kappa a\mu^2f_a^2}{2B}\left[1-\sqrt{1-4B\sin^2\left(\frac{\phi}{2f_a}\right)}\right]+\frac{ra\phi^2\omega^2}{2}+\frac{r}{2}\left(\frac{d\phi}{dr}\right)^2, \tag{2.9}$$

$$\frac{1}{a}\frac{da}{dr}=\frac{1-a}{r}+\frac{r\kappa a\mu^2f_a^2}{2B}\left[1-\sqrt{1-4B\sin^2\left(\frac{\phi}{2f_a}\right)}\right]+\frac{ra\phi^2\omega^2}{\alpha^2}+r\left(\frac{d\phi}{dr}\right)^2, \tag{2.10}$$

$$\frac{d^2\phi}{dr^2}=-\frac{a\phi\omega^2}{\alpha^2}+\left(\frac{d\phi}{dr}\right)\left[\left(\frac{1}{2a}\frac{da}{dr}\right)-\frac{2}{r}-\frac{1}{\alpha}\frac{d\alpha}{dr}\right]+\frac{a\sqrt{4\pi}\mu^2f_a}{\sqrt{1-4B\sin^2\left(\frac{\phi}{2f_a}\right)}}\sin\left(\frac{\phi}{f_a}\right). \tag{2.11}$$

To solve systems 2.9–2.11, one must choose appropriate boundary conditions, which are as follows. In order to guarantee that the spacetime is locally flat at the origin, the condition $a(0)=1$ is required. Furthermore, we ask for $\frac{d\phi(0)}{dr}=0$. Additionally, for solutions that represent an isolated configuration, the scalar field must vanish at infinity. In this limit, asymptotic flatness is reached. These conditions reduce the system to an eigenvalue problem for ω such that for each choice of $\phi_c=\phi(0)$, the system has a solution that decays exponentially at infinity. In order to solve the system numerically, it is convenient to use dimensionless quantities defined by

$$\bar{r}=\mu r,\quad \bar{\omega}=\frac{\omega}{\mu},\quad \bar{\phi}=\sqrt{\frac{\kappa}{2}}\phi,\quad \bar{\alpha}=\frac{\mu}{\omega}\alpha. \tag{2.12}$$

After substituting this scaling 2.12 in systems 2.9–2.11, the rescaled system is left in units of the mass parameter μ, which fixes the scale. Given a value of the field at the origin ϕ_c as a free parameter, we choose a trial value of the lapse and integrate the system outward from the origin using a fourth-order Runge–Kutta scheme with an adaptive step size. This adaptive scheme allowed us to reach smaller values of f_a. Then, we use a shooting algorithm to find the value of the lapse that corresponds to asymptotically flat solutions. We construct families of axion boson stars for different values of the parameter f_a and different values of the central scalar field. We also focus on solutions with no nodes in the scalar field corresponding to the ground state.

2.3 Diagnostic quantities

As demonstrated by Guerra et al. (2019), in the limit of large f_a, mini-boson stars are recovered, and this happens for values $f_a \sim \mathcal{O}(10)$, which, in physical units, corresponds to values of $f_a \sim 1.22 \times 10^{20}$GeV. In bosonic stars, the scalar field decays exponentially (since one asks for asymptotically flat spacetime), and consequently, they do not have a well-defined boundary; thus, it is common to describe their effective size in terms of the R_{99} radius, which is defined as the radius of the sphere containing 99% of the total mass of the star. In addition, we determine the star's compactness as $C = \frac{M}{R_{99}}$.

The energy density ρ, radial pressure p_r, and tangential pressure p_t are defined in terms of the stress–energy tensor 2.3 as

$$\rho = -T^t{}_t = \frac{1}{2}\left[\frac{\omega^2}{\alpha^2}\phi^2 + \frac{1}{a^2}(\partial_r\phi)^2\right] + \frac{1}{2}V(\phi), \tag{2.13}$$

$$p_r = T^r{}_r = \frac{1}{2}\left[\frac{\omega^2}{\alpha^2}\phi^2 + \frac{1}{a^2}(\partial_r\phi)^2\right] - \frac{1}{2}V(\phi), \tag{2.14}$$

$$p_t = T^\theta{}_\theta = T^\phi{}_\phi = \frac{1}{2}\left[\frac{\omega^2}{\alpha^2}\phi^2 - \frac{1}{a^2}(\partial_r\phi)^2\right] - \frac{1}{2}V(\phi). \tag{2.15}$$

The total mass of the object M is given by the limit $r \to \infty$ of the function

$$M(r) = 4\pi\int_0^r \tilde{r}^2\rho(\tilde{r})\,d\tilde{r}. \tag{2.16}$$

In our numerical calculations, we approach M as the value of this function evaluated at the outer point of the numerical grid. Alternatively, one can also find the total mass of the system by assuming that far away, the metric reduces to the Schwarzschild metric (Misner et al., 1973) so that

$$M = \lim_{r\to\infty}\frac{r}{2}\left(1 - \frac{1}{a^2}\right). \tag{2.17}$$

This expression converges very rapidly as r grows due to the exponential decay of the scalar field, and nonetheless, we checked that the results obtained with both expressions 2.16, 2.17 agree in the limit of large r.

3 Results

The periodic potential for the axion as given in Equation 2.7 is shown in Figure 1 for some representative values of f_a. Close to the minimum around $\phi \approx 0$, as the value of f_a increases, the quadratic behavior of the field dominates the potential and the solutions resemble the mini-boson stars. We show some results for the families of solutions corresponding to different values of f_a in the following.

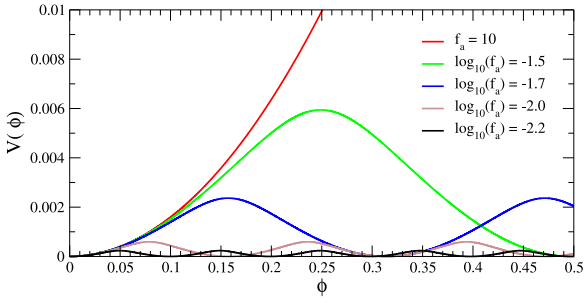

FIGURE 1
Periodic scalar field potential, as given in (2.7), for some values of the decaying constant f_a. For larger values of $f_a \sim 10$, the potential tends to a quadratic behavior. We consider $\mu = 1$; however, the potential can be rescaled with μ^2.

3.1 Families of solutions

It is known since the pioneer works of Kaup (1968) and Ruffini and Bonazzola (1969) that the mass of mini-boson stars has a maximum value $M_{\rm Kaup} = 0.633 m_{\rm Pl}^2/\mu$, where $m_{\rm Pl}$ represents the Planck mass. For $f_a = 10$, the system tends to the standard mini-boson star in which there is a local maximum at a critical value of ϕ_c that separates between stable and unstable configurations. This case is recovered for large values of f_a. Figure 2 displays the existence plots of the mass *versus* the central value of the field ϕ_c, for different configurations with some representative values of the decaying constant: $f_a = 10$ $\log_{10}(f_a) = -1.5$, $\log_{10}(f_a) = -1.7$, and $\log_{10}(f_a) = -2.0$. The top left panel shown in Figure 2 corresponds to this limiting behavior. However, smaller values of the decay constant f_a lead to the formation of new branches. Furthermore, when the numerical value of f_a decreases, finding solutions becomes more challenging from the numerical point of view, and in this work, we found solutions for values up to $\log_{10} f_a = -2.7$. As shown in Figure 3, as f_a decreases, the existence diagram becomes more intricate with several local maxima and minima. The existence of these local extreme points indicate new stability branches at higher densities, giving rise to radially stable boson stars. Furthermore, the compactness of such solutions increases when the value of f_a decreases.

For larger f_a, the solutions reduce to the standard mini-boson stars, but in the limit $f_a \to 0$, solutions with the appropriate boundary conditions, representing localized objects, are more difficult to find.

We now move to the description of the stars for a fixed value of f_a. For the sake of simplicity, we show the results for $\log_{10}(f_a) = -1.7$. Figure 4 shows the parametric plots of radial and tangential pressures $[p_r(r), p_t(r)]$ as given by (2.14 and 2.15. In the figure, the dashed line corresponds to the identity $p_r = p_t$. Larger deviations from this line, thus, correspond to larger anisotropy. The plots correspond to configurations marked with dots in Figure 2

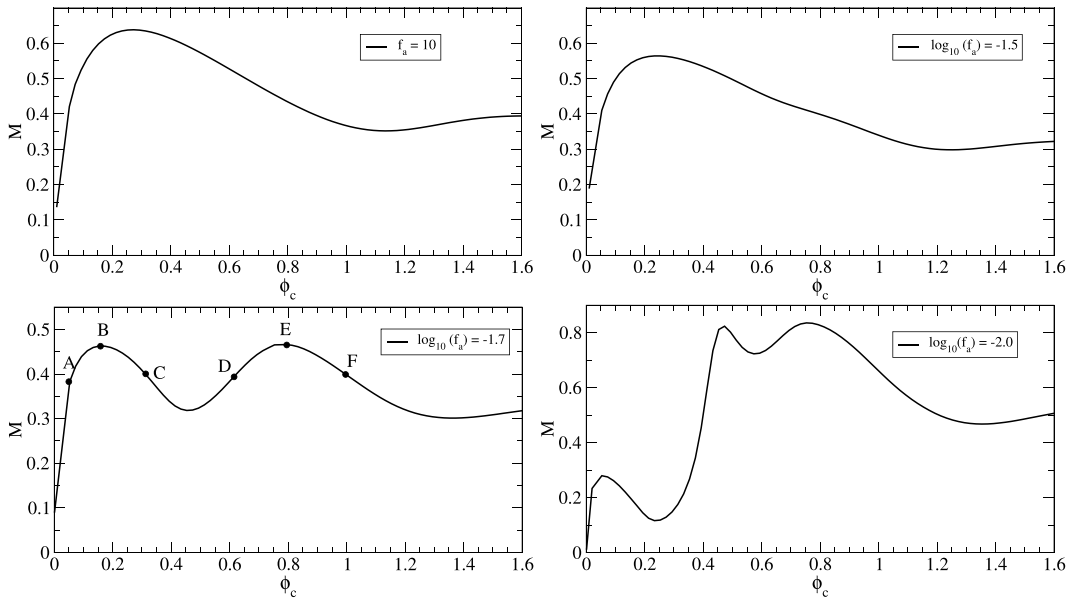

FIGURE 2
Existence plots. Each point on these curves corresponds to a solution of the Einstein-scalar field system. The local maxima separate the stable and unstable regions. The solutions with $f_a = 10$ are consistent with the mini-boson stars described by Kaup (1968). For smaller values of the decay constant f_a, a richer structure appears with more than one maximum and more than one minimum. The value of the maximum mass configurations increases as the value of f_a decreases.

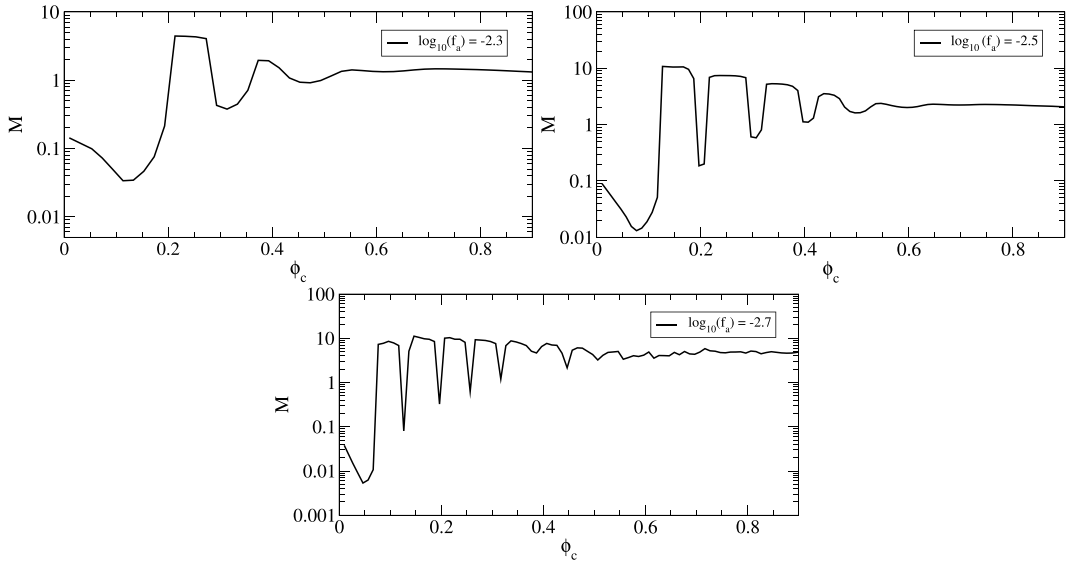

FIGURE 3
For smaller values of f_a, the existence plots develop several local maxima and minima.

and labeled with letters from A–F. Configuration A, with smaller values of ϕ_c, display only a small deviation from isotropy; however, as the value of ϕ_c increases, the stars become more anisotropic. For configuration E, the change of sign in the tangential pressure becomes more evident. However, the anisotropy is not as large as the one presented in other boson stars (Steven, 2012; Alcubierre et al., 2018; Alcubierre et al., 2019). The values of the radius, mass, and compactness for configurations A–F are listed in Table 1. As one moves to the right in the existence plot, with larger values of ϕ_c, axion stars become more compact. In the last column of Table 1, the numerical values of compactness are listed. As one moves to higher values of ϕ_c, the compactness increases. This trend is also present for the smaller values of f_a used in this work. Nonetheless, it seems that the compactness does not reach the maximum compactness

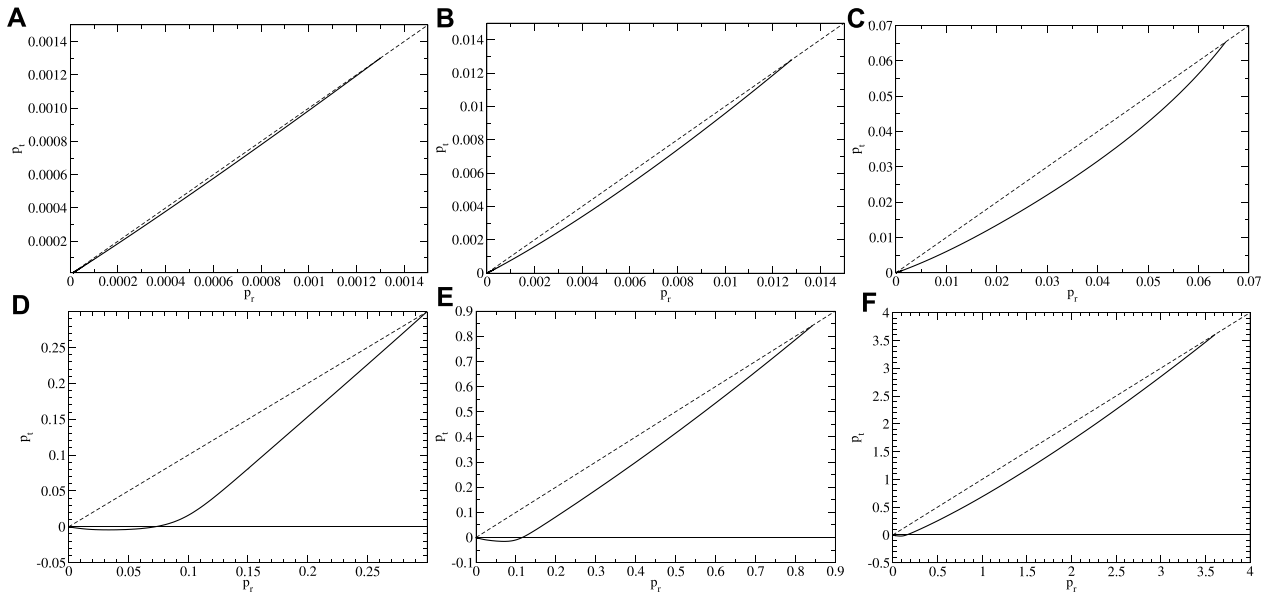

FIGURE 4
The measure of the anisotropy of axion stars is given by the difference between radial and tangential pressure. The dashed line represents the identity $p_t = p_r$. The configurations displayed correspond to the ones in the bottom panel of Figure 2 labeled from **(A–F)**.

TABLE 1 Parameters of the configurations shown in Figure 2 with $\log_{10}(f_a) = -1.7$: the value of the field at the origin, ϕ_c, the effective size as determined by the R_{99} radius, the total mass M, and the compactness.

Model	ϕ_c	R_{99}	M	C
A	0.05	79.070	0.38327	4.84731×10^{-3}
B	0.17	49.629	0.46259	9.32078×10^{-3}
C	0.30	39.740	0.39875	1.00340×10^{-2}
D	0.62	24.000	0.39312	1.63804×10^{-2}
E	0.80	22.640	0.46617	2.05906×10^{-2}
F	1.03	21.650	0.40107	1.85255×10^{-2}

limit (Buchdahl, 1966). Figure 5 displays the profiles of radial and tangential pressure as well as the density given in 2.13 of the configuration with the local maximum mass labeled as B and E in Figure 2. For configuration B, the difference in terms of absolute values between p_r and p_t is quite small. For configuration E, the same trend holds, but the tangential pressure becomes negative in the more exterior parts of the star. In both models, the maximum density is attained in the origin as in the usual mini-boson stars. Figure 5 shows the radial profiles of the metric coefficients α and a. In both models, the relation $a/\alpha \to 1$ holds at infinity, which is consistent with a Schwarzschild asymptotic behavior. In the more compact model E, a lower value of the lapse is attained at the origin, which is related with the fact that this configuration is more compact.

In general relativity, the maximum compactness of a self-gravitating, isotropic and spherically symmetric object made of a perfect fluid is $M/R = 4/9$, where M represents the mass of the object and R represents its radius. However, the above number, known as Buchdahl's bound, relies strongly on the hypothesis of isotropy (Buchdahl, 1966). Considerable effort has been dedicated to model the properties of anisotropic matter, with the hope of finding physically viable models of compact stars. While anisotropies are generally negligible as compared to the pressure, it has been shown that even small anisotropies in fluid stars may induce significant changes on the mass and compactness of the star (Raposo et al., 2019). To determine the structure of a compact star, a widely followed path is to specify an equation of state and then solve the field equations. Customarily, this is carried out considering hydrodynamical equilibrium; however, in this work, we found that moderate anisotropic configurations exist for the potential (2.7), yielding to highly compact objects. Nonetheless, our results indicate that for the axion periodic potential, it is not possible to surpass Buchdahl's bound.

3.2 Geodesic motion of test particles

It will also be helpful in identifying some general properties of the motion of test particles propagating in the spacetime associated with the previously found stars and, in particular, in determining whether the solutions admit stable circular orbits or light rings. The interest of studying light rings in compact objects has been renewed because of the correspondence between the quasi-normal modes of black holes and light ring oscillations to describe the initial part of the ringdown gravitational-wave signal of black holes (Cardoso et al., 2009; Cardoso and Pani, 2017; Khanna and Price, 2017).

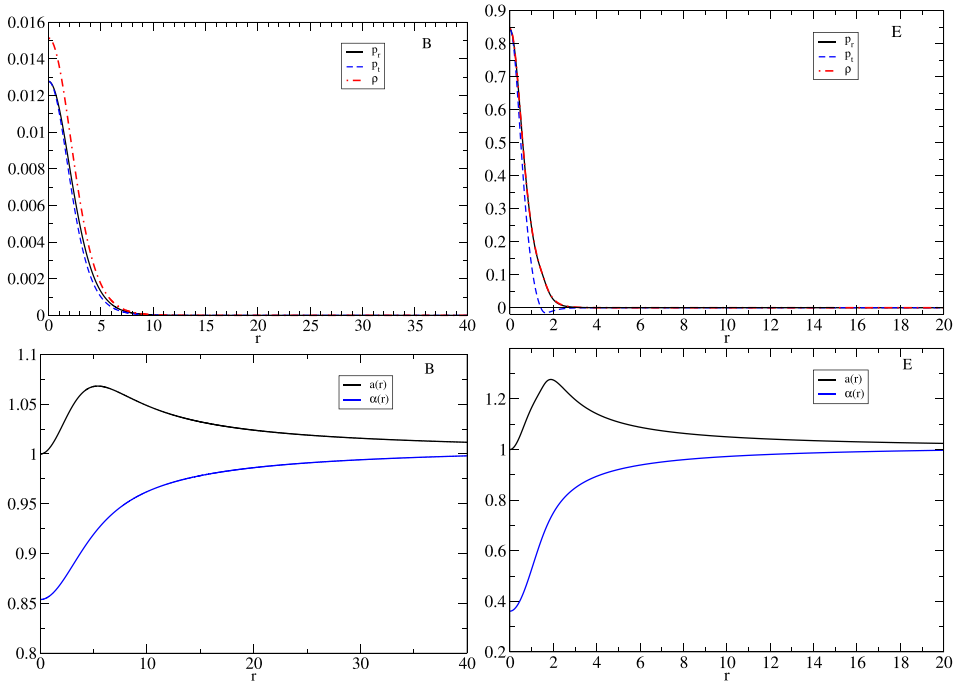

FIGURE 5
Top panels: energy density and radial and tangential pressure profiles for configurations B and E in Figure 2. These configurations correspond to local maximum masses. Bottom panels display the corresponding metric coefficient *a* and the lapse function α.

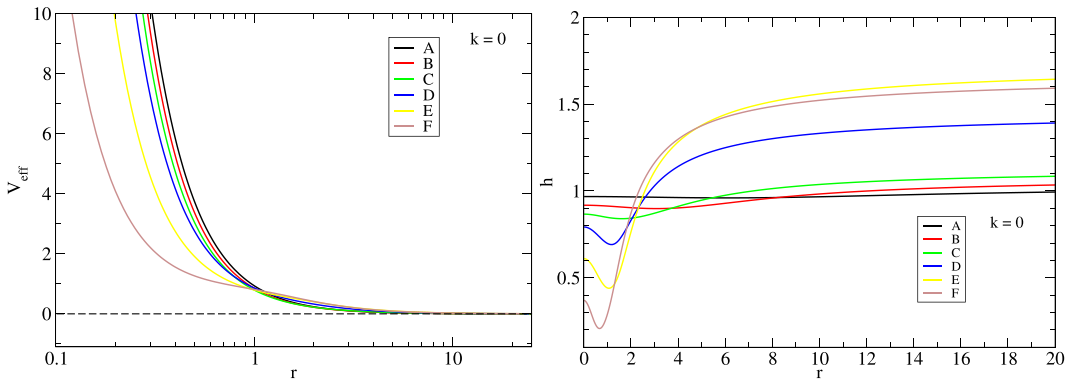

FIGURE 6
Left: effective potential (3.6) for null geodesics. Right: function $h(r) = \alpha - r\alpha\prime$. The zeroes of *h* determine the existence of light rings. For configurations A–F in Figure 2, there are no light rings.

In order to describe the motion of test particles in the spacetime (2.5), let us consider the Lagrangian equation as follows:

$$2\mathcal{L} = -\alpha^2 \dot{t}^2 + a^2 \dot{r}^2 + r^2 \dot{\theta}^2 + r^2 \sin^2\theta \dot{\varphi}^2, \tag{3.1}$$

where "dot" denotes the derivative with respect to the affine parameter τ. It is possible to consider $2\mathcal{L} = -k$ so that if $k = 1$, it corresponds to time-like geodesics and if $k = 0$, it corresponds to null geodesics.

Since the spacetime is spherically symmetric, we focus on particles in the plane $\theta = \pi/2$ in 3.1. Associated to the time and angular symmetry, there are two conserved quantities during the motion of the particles, namely, the energy at infinity E and the angular momentum ℓ given by

$$E = \frac{\partial \mathcal{L}}{\partial \dot{t}} = -\alpha^2 \dot{t}, \qquad \ell = \frac{\partial \mathcal{L}}{\partial \dot{\phi}} = r^2 \dot{\phi}. \tag{3.2}$$

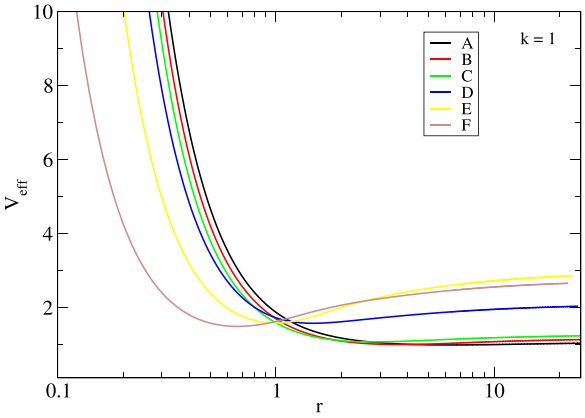

FIGURE 7
Effective potential for massive particles for the configurations A–F shown in Figure 2 with $\ell = 1$. The location of the minimum indicates the position of the circular orbit.

Normalization of the four velocities $u^\mu u_\mu = -k$ can be written in terms of the conserved quantities 3.2 yielding the equation

$$-k = -\frac{E^2}{\alpha^2} + a^2\dot{r}^2 + \frac{\ell^2}{r^2}, \tag{3.3}$$

Equation 3.3 can be written as

$$a^2\alpha^2\dot{r}^2 = E^2 - \alpha^2\left(k + \frac{\ell^2}{r^2}\right). \tag{3.4}$$

Defining a new variable z, through $\frac{dz}{dr} = a\alpha$, equation (3.4) becomes

$$\dot{z}^2 = E^2 - V_{\text{eff}}, \tag{3.5}$$

where the effective potential in 3.5 is defined as

$$V_{\text{eff}} = \alpha^2\left(k + \frac{\ell^2}{r^2}\right). \tag{3.6}$$

Circular motion of particles is possible when the conditions $\dot{r} = 0$ and $\frac{V_{\text{eff}}}{dr} = 0$ applied to 3.6 are fulfilled. In the time-like case, these conditions completely specify the energy and angular momentum to be

$$E^2 = \frac{\alpha^3}{\alpha - r\alpha'} \qquad \text{and} \qquad \ell^2 = \frac{\alpha' r^3}{\alpha - r\alpha'}, \tag{3.7}$$

where the prime denotes the derivative with respect to r. For null geodesics, the existence of circular orbits is given by the condition $h(r) = \alpha - r\alpha' = 0$ for which expressions (3.7) are undetermined. Moreover, it has been proven that regular configurations can have two light rings, of which one is stable (Pedro et al., 2017). However, not all configurations considered here admit light rings, and their appearance will depend on the compactness of the star. On the other hand, regarding massive particles, there always exist stable circular orbits. Figure 6 shows the potential (3.6) for null geodesics (with $k = 0$) for configurations A to F in Figure 2 with $\log_{10}(f_a) = -1.7$. For this value of f_a, configurations are not compact enough to have light rings. Since the potential for these configurations is very alike, the motion of null particles around them is quite similar. In the right panel of Figure 6, the function $h(r)$ is displayed, and the change of behavior close the origin for configurations D–F is observed, and there is a slight decay on the value of $h(r)$. It can be seen in the figure that as the configurations become more compact, h decreases in such a way that it will cross the origin twice, giving rise to the existence of a pair of light rings. For configurations with lower values of $\log_{10}(f_a) \approx -2.3$, this is actually the case, and a pair of light rings appear. Figure 7 displays the effective potential for massive particles ($k = 1$) with $\ell = 1$ for configurations A–F. In all cases, the potential is minimum, indicating the existence of circular orbits.

4 Final remarks

In this work, we considered solutions to the spherically symmetric stationary Einstein-axion field system known as axion stars, which have been previously studied by Guerra et al. (2019). This system is characterized because the scalar field potential is periodic on the field. We presented solutions with no nodes on the scalar field (also known as ground state solutions) varying the value of the axion decay constant f_a. Axion stars with $f_a \gg \phi$ have similar properties as mini-boson stars in the sense that they have a local maximum of the total mass M for a finite value of the central value of the field ϕ_c. As the value of the constant f_a decreases, more local maxima appear, and it is possible to find solutions with larger values of mass with larger values of ϕ_c. However, as a consequence, local minima also appear, leading to a different region of stability. For smaller values of f_a, it becomes extremely difficult to find solutions since the system is quite sensible to the values of ϕ_c. Configurations with larger values of ϕ_c present larger anisotropies in the sense that the ratio between the tangential and radial pressures p_t/p_r differs slightly from unity. Furthermore, for values of ϕ_c beyond the first maximum in the mass, solutions with negative tangential pressure are found. Finally, regarding the motion of test particles, stars with small values of f_a may have high compactness that allow the existence of light rings, while for time-like particles, the existence of circular orbits is possible. This characteristic may be used to explore the astrophysical features of axion stars.

Author contributions

BB: writing–original draft and writing–review and editing. JD: writing–original draft and writing–review and editing.

Funding

The authors declare that financial support was received for the research, authorship, and/or publication of this article. This work was partially supported by DGAPA-UNAM through grant IN110523, by the CONACyT Network Project No. 376127 “Sombras, lentes y ondas gravitatorias generadas por objetos compactos astrofisicos,” and No. 304001 “Estudio de campos

escalares con aplicaciones en cosmología y astrofísica," and by the European Union's Horizon 2020 research and innovation (RISE) program H2020-MSCARISE- 2017, Grant No. FunFiCO-777740, and the European Horizon Europe staff exchange (SE) program HORIZONMSCA- 2021-SE-01, Grant No. NewFunFiCO-101086251.

Conflict of interest

The authors declare that the research was conducted in the absence of any commercial or financial relationships that could be construed as a potential conflict of interest.

Publisher's note

All claims expressed in this article are solely those of the authors and do not necessarily represent those of their affiliated organizations, or those of the publisher, the editors, and the reviewers. Any product that may be evaluated in this article, or claim that may be made by its manufacturer, is not guaranteed or endorsed by the publisher.

References

Alcubierre, M., Barranco, J., Bernal, A., Degollado, J. C., Diez-Tejedor, A., Megevand, M., et al. (2018). *Cl. Quant. Grav.* 35 (19), 19LT01. doi:10.1088/1361-6382/aadcb6

Alcubierre, M., Barranco, J., Bernal, A., Degollado, J. C., Diez-Tejedor, A., Megevand, M., et al. (2019). Dynamical evolutions of ℓ-boson stars in spherical symmetry. *Cl. Quant. Grav.* 36 (21), 215013. doi:10.1088/1361-6382/ab4726

Alcubierre, M., Becerril, R., Guzman, S. F., Matos, T., Nunez, D., and Arturo Urena-Lopez, L. (2003). Numerical studies of Phi * *2 oscillatons. *Cl. Quant. Grav.* 20, 2883–2904. doi:10.1088/0264-9381/20/13/332

Alexander, K., and Shaposhnikov, M. E. (1998). Supersymmetric Q balls as dark matter. *Phys. Lett. B* 418, 46–54. doi:10.1016/s0370-2693(97)01375-0

Arturo Ureña-López, L., and Matos, T. (2000). New cosmological tracker solution for quintessence. *Phys. Rev.* D62, 081302. doi:10.1103/PhysRevD.62.081302

Arvanitaki, A., Dimopoulos, S., Dubovsky, S., Kaloper, N., and March-Russell, J. (2010). String Axiverse. *Phys. Rev.* D81, 123530. doi:10.1103/physrevd.81.123530

Arvanitaki, A., and Dubovsky, S. (2011). Exploring the string Axiverse with precision black hole physics. *Phys. Rev.* D83, 044026. doi:10.1103/physrevd.83.044026

Brito, R., Cardoso, V., CarlosHerdeiro, A. R., and Radu., E. (2016). Proca stars: gravitating Bose–Einstein condensates of massive spin 1 particles. *Phys. Lett. B* 752, 291–295. doi:10.1016/j.physletb.2015.11.051

Brito, R., Cardoso, V., and Pani, P. (2015). Superradiance: new Frontiers in black hole physics. *Lect. Notes Phys.* 906, 1–237. doi:10.1007/978-3-030-46622-0

Buchdahl, H. A. (1966). General relativistic fluid spheres. II. General inequalities for regular spheres. *Astrophys. J.* 146, 275. doi:10.1086/148875

Cardoso, V., Miranda, A. S., Berti, E., Witek, H., and Vilson, T. Z. (2009). Geodesic stability, Lyapunov exponents and quasinormal modes. *Phys. Rev. D.* 79 (6), 064016. doi:10.1103/physrevd.79.064016

Cardoso, V., and Pani, P. (2017). Tests for the existence of black holes through gravitational wave echoes. *Nat. Astron* 1 (9), 586–591. doi:10.1038/s41550-017-0225-y

Caso, C., Conforto, Gurtu, A., Aguilar-Benitez, M., Amsler, C., Barnett, R. M., et al. (2018). Review of particle physics. *Phys. Rev. D.* 98 (3), 030001–030783. doi:10.1007/s10052-998-0104-x

Colpi, M., Shapiro, S. L., and Wasserman, I. (1986). Boson stars: gravitational equilibria of self-interacting scalar fields. *Phys. Rev. Lett.* 57, 2485–2488. doi:10.1103/physrevlett.57.2485

Delgado, J. F. M., Herdeiro, C. A. R., and Radu., E. (2020). Rotating axion boson stars. *JCAP* 06. 037. doi:10.1088/1475-7516/2020/06/037

Di Giovanni, F., Guerra, D., Albanesi, S., Miravet-Tenés, M., and Tseneklidou, D. (2022). Fermion-axion stars: static solutions and dynamical stability. *Phys. Rev. D.* 106 (8), 084013. doi:10.1103/physrevd.106.084013

Di Luzio, L., Giannotti, M., Nardi, E., and Visinelli, L. (2020). The landscape of QCD axion models. *Phys. Rept.* 870, 1–117. doi:10.1016/j.physrep.2020.06.002

Enqvist, K., and McDonald, J. (1998). Q balls and baryogenesis in the MSSM. *Phys. Lett. B* 425, 309–321. doi:10.1016/s0370-2693(98)00271-8

Graham, P. W., Irastorza, I. G., Lamoreaux, S. K., Lindner, A., and van Bibber, K. A. (2015). Experimental searches for the axion and axion-like particles. *Ann. Rev. Nucl. Part. Sci.* 65, 485–514. doi:10.1146/annurev-nucl-102014-022120

Guerra, D., CaioMacedo, F. B., and Pani, P. (2019). Axion boson stars. *JCAP* 09 (09), 061. [Erratum: JCAP 06, E01 (2020)]. doi:10.1088/1475-7516/2019/09/061

Herdeiro, C., Perapechka, I., Radu, E., and Shnir, Ya. (2019). Asymptotically flat spinning scalar, Dirac and Proca stars. *Phys. Lett. B* 797, 134845. doi:10.1016/j.physletb.2019.134845

Jetzer, P. (1992). Boson stars. *Phys. Rept.* 220, 163–227. doi:10.1016/0370-1573(92)90123-h

Kaup, D. J. (1968). Klein-gordon geon. *Phys. Rev.* 172, 1331–1342. doi:10.1103/physrev.172.1331

Khanna, G., and Price, R. H. (2017). Black hole ringing, quasinormal modes, and light rings. *Phys. Rev. D.* 95 (8), 081501. doi:10.1103/physrevd.95.081501

Lam, H., Ostriker, J. P., Scott, T., and Witten, E. (2017). Ultralight scalars as cosmological dark matter. *Phys. Rev.* D95 (4), 043541. doi:10.1103/PhysRevD.95.043541

Marsh, D. J. E. (2016). Axion cosmology. *Phys. Rept.* 643, 1–79. doi:10.1016/j.physrep.2016.06.005

Marsh, D. J. E., and Ferreira, P. G. (2010). Ultra-light scalar fields and the growth of structure in the universe. *Phys. Rev.* D82, 103528. doi:10.1103/physrevd.82.103528

Marsh, D. J. E., and Pop, A.-R. (2015). Axion dark matter, solitons and the cusp?core problem. *Mon. Not. Roy. Astron. Soc.* 451 (3), 2479–2492. doi:10.1093/mnras/stv1050

Marsh, D. J. E., and Silk, J. (2014). A model for halo formation with axion mixed dark matter. *Mon. Not. Roy. Astron. Soc.* 437 (3), 2652–2663. doi:10.1093/mnras/stt2079

Matos, T., and Arturo Urena-Lopez, L. (2000). Quintessence and scalar dark matter in the universe. *Cl. Quantum Grav.* 17, L75–L81. doi:10.1088/0264-9381/17/13/101

Matos, T., and Arturo Urena-Lopez, L. (2001). A further analysis of a cosmological model of quintessence and scalar dark matter. *Phys. Rev.* D63, 063506. doi:10.1103/PhysRevD.63.063506

Matos, T., and Arturo Urena-Lopez, L. (2002). Scalar field dark matter, cross section and Planck-scale physics. *Phys. Lett.* B538, 246–250. doi:10.1016/s0370-2693(02)02002-6

Matos, T., and Arturo Urena-Lopez, L. (2007). Flat rotation curves in scalar field galaxy halos. *Gen. Rel. Grav.* 39, 1279–1286. doi:10.1007/s10714-007-0470-y

Matos, T., Bernal, A., and Núñez, D. (2008). Flat central density profiles from scalar field dark matter halo. *Rev. Mex. A. A* 44, 149.

Matos, T., Guzman, F. S., and Arturo Urena-Lopez, L. (2000). Scalar field as dark matter in the universe. *Cl. Quantum Grav.* 17, 1707–1712. doi:10.1088/0264-9381/17/7/309

Mielke, E. W., and Scherzer, R. (1981). Mielke and reinhard scherzer. Geon-Type solutions of the nonlinear heinsenberg-klein-gordon equation. *Phys. Rev.* D24, 2111–2126. doi:10.1103/PhysRevD.24.2111

Mielke, E. W., and Schunck, F. E. (2000). Boson stars: alternatives to primordial black holes? *Nucl. Phys.* B564, 185–203. doi:10.1016/s0550-3213(99)00492-7

Misner, C. W., Thorne, K. S., and Wheeler, J. A. (1973). *Gravitation*. San Francisco: Academic Press.

Peccei, R. D., and Quinn, H. R. (1977). Cp conservation in the presence of pseudoparticles. *Phys. Rev. Lett.* 38, 1440–1443. doi:10.1103/physrevlett.38.1440

Pedro, V. P. C., Emanuele, B., and Herdeiro, C. A. R. (2017). Light-ring stability for ultracompact objects. *Phys. Rev. Lett.* 119 (25), 251102. doi:10.1103/physrevlett.119.251102

Porayko, N. K., and Postnov, K. A. (2014). Constraints on ultralight scalar dark matter from pulsar timing. *Phys. Rev. D.* 90 (6), 062008. doi:10.1103/physrevd.90.062008

Raposo, G., Pani, P., Bezares, M., Palenzuela, C., and Cardoso, V. (2019). Anisotropic stars as ultracompact objects in General Relativity. *Phys. Rev. D.* 99 (10), 104072. doi:10.1103/physrevd.99.104072

Ruffini, R., and Bonazzola, S. (1969). Systems of self-gravitating particles in general relativity and the concept of an equation of state. *Phys. Rev.* 187, 1767–1783. doi:10.1103/physrev.187.1767

Schive, H.-Yu, Chiueh, T., and Broadhurst, T. (2014). Cosmic structure as the quantum interference of a coherent dark wave. *Nat. Phys.* 10, 496–499. doi:10.1038/nphys2996

Seidel, E., and Suen, W.-Mo (1990). Dynamical evolution of boson stars: perturbing the ground state. *Phys. Rev. D.* 42, 384–403. doi:10.1103/physrevd.42.384

Seidel, E., and Suen, W. M. (1991). Oscillating soliton stars. *Phys. Rev. Lett.* 66, 1659–1662. doi:10.1103/physrevlett.66.1659

Sikivie, P. (2014). Axion dark matter detection using atomic transitions. *Phys. Rev. Lett.* 113 (20), 201301. [Erratum: Phys.Rev.Lett. 125, 029901 (2020)]. doi:10.1103/physrevlett.113.201301

Steven, L. (2012). Liebling and carlos palenzuela. Dynamical boson stars. *Living Rev. Rel.* 15 (6). doi:10.1007/s41114-017-0007-y

Zeng, Y.-Bo, Li, H.-Bo, Sun, S.-X., Cui, S.-Y., and Wang, Y.-Q. (2021). Rotating hybrid axion-miniboson stars. 3 Available at: https://arxiv.org/abs/2103.10717.

Zeng, Y.-Bo, Sun, S.-X., Cui, S.-Y., Zhang, Y.-P., and Wang, Y.-Q. (2023). Rotating multistate axion boson stars. 9 Available at: https://arxiv.org/abs/2309.05743.